change in the past. However, historical climate changes were generally much slower (by one or more orders of magnitude) than those predicted for the future (*23, 24*). Slower changes may have provided opportunities for taxa to adapt to climate change while persisting in refuges or shifting ranges to new latitudes despite genetic constraints on adaptive evolution.

References and Notes

1. M. B. Davis, R. G. Shaw, *Science* **292**, 673 (2001).
2. M. J. Groom, N. Schumaker, in *Biotic Interactions and Global Change*, P. M. Kareiva *et al.*, Eds. (Sinauer, Sunderland, MA, 1993).
3. N. Shigesada, K. Kawasaki, *Biological Invasions: Theory and Practice* (Oxford Univ. Press, Oxford, 1997).
4. J. Antonovics, *Ann. Mo. Bot. Gard.* **63**, 224 (1976).
5. R. Lande, *Evolution* **33**, 402 (1979).
6. The locations of the natural populations were as follows. MN: Kellog-Weaver dunes, Wabasha County, Minnesota; KS: Konza Prairie, Riley County, Kansas; OK: Pontotoc Ridge, Pontotoc County, Oklahoma. *C. fasciculata* is an native annual legume that has limited dispersal; the estimated neighborhood area based on seed and pollen disperal is 16.7 m^2 [C. B. Fenster, *Evolution* **45**, 398 (1991)].
7. J. R. Etterson, thesis, University of Minnesota, St. Paul, MN (2000).
8. Data from model CGCM1 of the Canadian Climate Center are available at www.cccma.bc.ec.gc.ca/models/cgcm1.shtml, manipulated by VEMAP2. An overview from T. Kittel *et al.*, ("VEMAP Phase II: Overview of VEMAP2 Gridded Climate Time Series for the U.S. National Assessment") is available at www.cgd.ucar.edu/vemap/V2.html (1999).
9. Field-collected seeds were grown under greenhouse conditions and crossed within populations according to nested paternal half-sib crossing designs, with three randomly chosen dams mated to each sire. Forty-eight half-sib families (144 full-sib) were produced within the MN population, 45 half-sib families (135 full-sib) within KS, and 50 half-sib (150 full-sib) within OK.
10. In spring 1998, pedigreed seeds, planted and reared in a greenhouse at the University of Minnesota for 3 weeks, were transplanted into field sites. For the OK site, seeds were planted 1 May and seedlings were transplanted 19 to 21 May at the Robert S. Kerr Environmental Research Center (Ada, OK). For the KS site, seeds were planted 6 May and transplanted 25 to 27 May at the Konza Prairie Research Natural Area (Manhatten, KS). For the MN site, seeds were planted 13 May and transplanted 30 May to 1 June at the University of Minnesota (St. Paul, MN). The planting design (four blocks per site and two replicates of each full-sib family per block) was not fully balanced because of germination failure, seedling mortality in the greenhouse, and planting errors (total plant numbers: MN = 3247, KS = 3360, and OK = 3301). At all sites, seedlings were watered for 5 days after transplantation. The OK site was weeded in June; the KS and MN sites were weeded in July and August. Few plants were damaged by deer (OK, 3.1%; KS, 1.2%). Another 1.9% of the plants at the OK site were lost due to vandalism. Palmer's drought severity index indicated that the climate in MN was drier than normal during the full growing season, KS was dry in April and May but near normal for the rest of the growing season, and OK had drought conditions beginning in April that became severe from July to September and had a record number of consecutive days over 37.8°C.
11. Phenological stages were as follows. 0, died before reproduction; 1, vegetative plant; 2, flowering plant without pods; 3, plant with developing green pods; 4, plant with ripening brown pods; and 5, senescent plant. Leaf thickness (specific leaf area) is leaf area (m^2) divided by dry leaf weight (g).
12. Fecundity is average seed count of three collected pods times total pod number. In cases where seed counts were not available because pods had already dehisced, fecundity was estimated using the average seed count of the other full-sib replicate within the block or, if that was not available, the average seed count of the full-sib family across blocks.
13. R. G. Shaw, *Evolution* **41**, 812 (1987).
14. R. G. Shaw, F. H. Shaw, Quercus programs published electronically, available via anonymous ftp from evolution.umn.edu, directory path pub/quercus (1994).
15. Variance components were restricted to the feasible parameters space (greater than zero). Signficance testing of Cov_{Aij} was done by calculating the log-likelihood ratio (LRT) and testing it against a chi-square distribution with one degree of freedom. $LRT = -2(L_o - L_{max})$, where L_o is the log likelihood of the null hypothesis that $Cov_{Aij} = 0$, and L_{max} is the log likelihood of the full model. LRT is distributed asymptotically as a chi square with r degress of freedom, where r is the number of parameters specified under the null hypothesis. To conform to the assumptions of multivariate normality, fecundity was log-transformed. Normality was assessed by visual inspection of normal probability plots of residuals from nested analysis of variance (ANOVA) for each population and site combination. Fecundity estimates of zero, which reflect plant death or unsuccessful reproduction, were retained despite distributional problems that they induced, because these observations reflect the process of natural selection. For plants in each population-site combination, fecundity was converted to relative fitness by dividing by the corresponding site- and population-mean fecundity. All other traits were log-transformed except for reproductive stage, where transformation did not improve the fit to normality. To account for patterns of environmental variation within the field plots, block and row within block were included as categorical factors in the models and position within row was included as a continuous covariate in all analyses.
16. A. Robertson, *Anim. Prod.* **8**, 95 (1968).
17. G. R. Price, *Nature* **227**, 520 (1970).
18. R. Lande, S. J. Arnold, *Evolution* **37**, 1210 (1983).
19. T. Mitchell-Olds, R. G. Shaw, *Evolution* **41**, 1149 (1987).
20. N. H. Barton, M. Turelli, *Annu. Rev. Genet.* **23**, 337 (1989).
21. S. Kalisz, *Evolution* **40**, 470 (1986).
22. C. A. Kelly, *Evolution* **46**, 1658 (1992).
23. B. Huntly, W. Cramer, A. V. Morgan, H. G. Prentic, J. R. M. Allen, in *Past and Future Rapid Environmental Changes: The Spatial and Evolutionary Responses of Terrestrail Biota*, B. Huntley *et al.*, Eds. (Springer-Verlag, Berlin, 1997).
24. K. V. Walker, M. B. Davis, S. Sugita, personal communication.
25. R. S. Thompson *et al.*, U.S. Geological Survey Professional Paper, 1650 A-B (2000).
26. ANOVA test statistics for the population factor (block and row position nested within block are not shown) for each site and trait, corresponding to Fig. 3, are as follows (***$P < 0.001$). (A) Seed number: MN site $F_{2,3288} = 240$ ***; KS site $F_{2,3235} = 563$ ***; OK site $F_{2,3252} = 544$ ***. (B) Reproductive stage: MN site $F_{2,2489} = 720$ ***; KS site $F_{2,2527} = 474$ ***; OK site $F_{2,3354} = 1187$ ***. (C) log (Leaf number): MN site $F_{2,2323} = 89$ ***; KS site $F_{2,2484} = 367$ ***; OK site $F_{2,3280} = 595$ ***. (D) log (Leaf thickness g m^{-2}): MN site $F_{2,3051} = 110$ ***; KS site POP $F_{2,3221} = 529$ ***; OK site $F_{2,3190} = 510$.

27. We thank F. Shaw for statistical advice and programming; S.-M. Chang and M. B. Davis for encouragement and comments on the manuscript; the Minnesota and Oklahoma Chapters of the Nature Conservancy and staff at the Konza Prairie Scientific and Natural Area and the Robert S. Kerr Environmental Research Center for logistical support; and M. Etterson, D. Otterson, R. Otterson, A. Mertyl, J. Larson, L. Kinsell, and T. Nguyen for field work. Supported by U.S. Environmental Protection Agency STAR fellowship U 914758-01-2, the Minnesota Center for Community Genetics, the Dayton-Wilkie Funds for Natural History, and the graduate school of the University of Minnesota.

21 June 2001; accepted 14 August 2001

Direct Interaction of *Arabidopsis* Cryptochromes with COP1 in Light Control Development

Haiyang Wang,[1] Li-Geng Ma,[1,2] Jin-Ming Li,[3] Hong-Yu Zhao,[3] Xing Wang Deng[1,2]*

Arabidopsis seedling photomorphogenesis involves two antagonistically acting components, COP1 and HY5. COP1 specifically targets HY5 for degradation via the 26*S* proteasome in the dark through their direct physical interaction. Little is known regarding how light signals perceived by photoreceptors are transduced to regulate COP1. *Arabidopsis* has two related cryptochromes (cry1 and cry2) mediating various blue/ultraviolet-A light responses. Here we show that both photoactivated cryptochromes repress COP1 activity through a direct protein-protein contact and that this direct regulation is primarily responsible for the cryptochrome-mediated blue light regulation of seedling photomorphogenic development and genome expression profile.

Arabidopsis uses two major types of photoreceptors, the red/far-red light-absorbing phytochromes (phyA-phyE) and two related blue/ultraviolet-A (UV-A)–absorbing cryptochromes (cry1 and cry2) to monitor the ambient light environment and to control the seedling developmental pattern, photomorphogenesis in the light and skotomorphogenesis in darkness (*1*, *2*). Previous studies showed that a group of COP/DET/FUS proteins function as repressors of photomorphogenesis (*3*–*5*). They achieve their roles by

mediating the regulated proteolysis of key developmental regulators, such as HY5, a bZIP transcription factor that promotes the expression of light-inducible genes and thus photomorphogenic development (*6–9*). However, little is known as to how the light-activated photoreceptors regulate the activities of these COP/DET/FUS proteins to cause the physiological responses.

It was recently reported that overexpression of GUS fusion proteins with the COOH-terminus of either CRY1 (GUS-CCT1, amino acids 490 to 681) or CRY2 (GUS-CCT2, amino acids 486 to 612) in *Arabidopsis* confers a constitutive light response in darkness (*10*), suggesting that the activities of some of the COP/DET/FUS proteins might be repressed in the dark. To examine whether direct protein-protein interactions between CCTs and the COP/DET/FUS proteins are involved in this repression, we subcloned CCT1 and CCT2, either by themselves or as fusions with the GUS protein (GUS-CCT1 and GUS-CCT2) into the yeast two-hybrid vectors (*11*), in both the LexA DNA binding domain and the GAL4 activation-domain (AD) fusion configurations. Yeast two-hybrid interaction assays of CCTs or GUS-CCTs with all available subunits of the COP9 signalosome (*11*) failed to detect any substantial protein-protein interaction in either configuration. However, clear interactions between both LexA-CCT2 and LexA-GUS-CCT2 with AD-COP1 were detected (Fig. 1A). Further domain deletion analysis revealed that LexA-CCT2 is capable of interacting with COP1 mutants lacking either the Ring-finger or the Coil domain, but not with COP1 mutants missing either the WD-40 repeat (G_β) domain or both the Ring-finger and Coil domains. LexA-GUS-CCT2 is capable of interacting with all of the COP1 deletion forms as long as they maintain the intact WD-40 repeat domain (Fig. 1A). This result suggests that the COOH-terminal WD-40 repeat domain is likely responsible for interacting with CCT2. The GUS protein–mediated oligomerization seems able to partially fulfill the structural role of the Coil domain of COP1.

To confirm the direct interaction between CRY2 and COP1 in vivo, we performed a coimmunoprecipitation assay. As shown in Fig. 1B, CRY2 antibodies can immunoprecipitate both CRY2 and COP1 with *Arabidopsis* transgenic seedlings overexpressing COP1 (COP1OE) (*12*) but not with samples that were processed without adding the CRY2 antibody or samples of the *cry2-1* mutant seedlings (*13*).

Our attempt to examine the interaction between CRY1 and COP1 with the above approaches was hampered by the self-activation property of CCT1 in yeast and the unavailability of a suitable CRY1 antibody. Instead, we selected a living onion cell colocalization assay (*14*) for this purpose. As shown in Fig. 2, GFP-CCT1 alone ex-

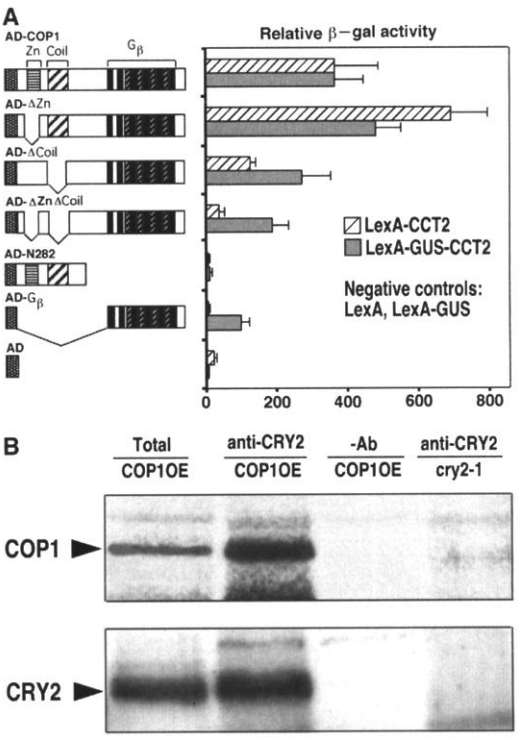

Fig. 1. Analysis of CRY2 and COP1 interaction in yeast and in planta. (**A**) CCT2 and COP1 interaction analyzed by the yeast two-hybrid assay. The left panel illustrates the AD-COP1 fusion constructs. Zn, Ring-finger domain; Coil, Coiled-coil domain; G_β, WD-40 repeat domain; N282, NH_2-terminal 282–amino acid fragment of COP1. The right panel shows the corresponding β-galactosidase activities with either LexA-CCT2 or LexA-GUS-CCT2. The value is the average of six individual yeast colonies, and the error bars represent the standard deviations (*15*). (**B**) Coimmunoprecipitation of CRY2 and COP1 in vivo. The top and bottom panels show Western blot analysis of immunoprecipitated (with or without CRY2 antibody added) samples probed with COP1 antibodies or CRY2 antibodies, respectively. "Total" indicates total protein extracts not subjected to immunoprecipitation. COP1OE, COP1 overexpressing *Arabidopsis* seedlings; *cry2-1*, CRY2 mutant *Arabidopsis* seedlings. −Ab indicates samples processed without adding the CRY2 antibody (*15*).

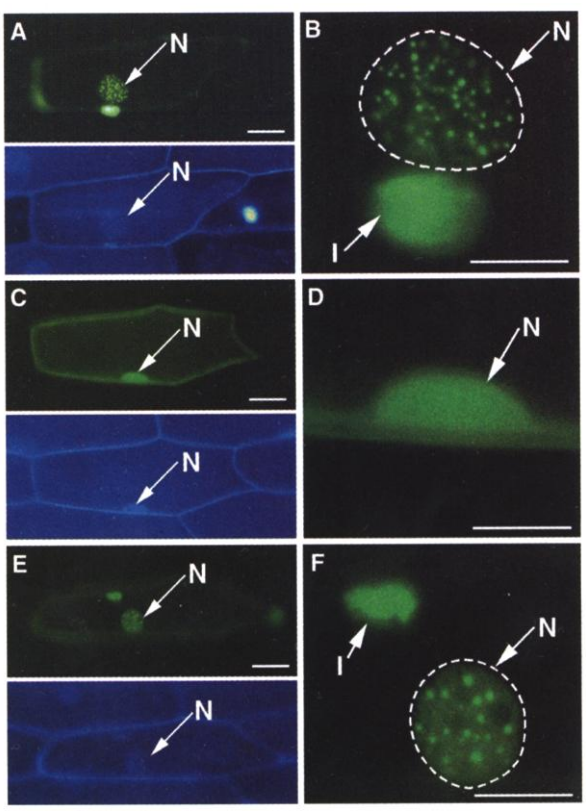

Fig. 2. Recruitment of GFP-CCT1 into COP1 nuclear speckles and cytoplasmic inclusion bodies in living plant cells. (**A**), (**C**), and (**E**) are composed of two portions: The top panels show the fluorescent images of GFP-COP1, GFP-CCT1, or GFP-CCT1 coexpressing with a nontagged COP1 in living onion epidermal cells; the bottom panels are DAPI (4′,6′-diamidino 2-phenylindole) staining of the same images to show the positions of the nuclei (indicated by arrows). (**B**), (**D**), and (**F**) are closeups of the nuclei as shown in (A), (C), and (E), respectively (*15*). Dashed lines demarcate the nuclei. N, nucleus; I, cytoplasmic inclusion body. The scale bar in all panels represents 50 μm.

[1]Department of Molecular, Cellular, and Developmental Biology, Yale University, New Haven, CT 06520, USA. [2]Peking-Yale Joint Center of Plant Molecular Genetics and Agrobiotechnology, College of Life Sciences, Peking University, Beijing 100871, People's Republic of China. [3]Department of Epidemiology and Public Health, Yale University School of Medicine, New Haven, CT 06520, USA.

*To whom correspondence should be addressed. E-mail: xingwang.deng@yale.edu

hibited a uniform green fluorescent pattern enriched in the nucleus. Its coexpression with a nontagged COP1 resulted in bright green nuclear speckles over the uniform green fluorescent background as well as strong green fluorescent cytoplasmic inclusion bodies. Both are characteristic features of COP1 and its GFP fusion. This result demonstrates that GFP-CCT1 can be recruited into both the nuclear speckles and the cytoplasmic inclusion bodies of COP1, supporting a direct interaction between CRY1 and COP1 in living plant cells.

It has been proposed that COP1 functions as a putative E3 ubiquitin ligase responsible for the targeted degradation of HY5 through the 26*S* proteasome (*8*). The observed physical interaction between cryptochromes and COP1 prompted us to postulate that COP1 is a direct signaling target for both cryptochromes in *Arabidopsis* (Web fig. 1) (*15*). It is conceivable that the blue light signals drive a redox reaction within cryptochromes to activate the CCTs, as a result of change in either the conformation or chemical property of CCTs, which leads to the rapid inactivation of COP1 through the direct protein-protein contact. This rapid inactivation of COP1 abrogates the targeted degradation of the downstream bZIP transcription factor HY5 and other substrates, which directly control light-responsive gene expression and the photomorphogenic development program (*6*, *16*). The long-term inactivation of COP1 is achieved by subsequent depletion of COP1 from the nucleus (*17*).

This model is consistent with the previous findings that both CRY1 and CRY2 mediate blue light–induced photomorphogenic development, characterized by shortening of the hypocotyl, cotyledon expansion, and anthocyanin production (*18*, *19*). Further, transgenic *Arabidopsis* seedlings overexpressing either photoreceptor are hypersensitive to blue light and exhibit enhanced light-induced shortening of the hypocotyl and increased anthocyanin synthesis (*13*, *20*). In addition, it has been demonstrated that both CRY1 and CRY2 mediate HY5 accumulation in blue light (*8*). These observations suggest that both cryptochromes contribute to blue light regulation of COP1 activity in a coordinated and quantitative manner.

The antagonistic relationship between cryptochromes and COP1 in mediating photomorphogenic development is further reinforced by a genetic study in which we introduced a COP1 overexpressing cassette into the *cry1* mutant (*21*) and the CRY1 overexpressing (*20*) backgrounds by genetic crossing. Figure 3, A and B, shows that overexpressing COP1 (COP1OE) in a wild-type background substantially reduces the extent of photomorphogenic development and the seedlings display elongated hypocotyls under

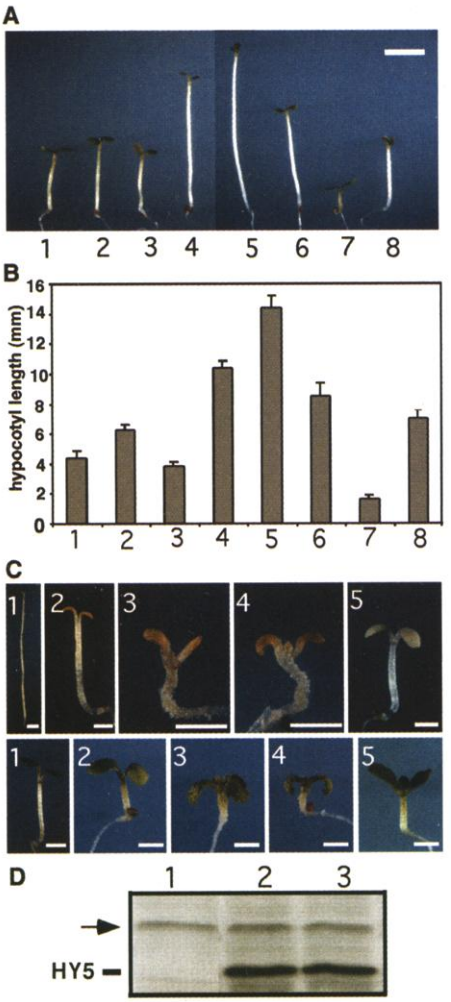

Fig. 3. Functional analysis of cryptochromes and COP1 interaction. (**A**) A combinatorial effect of the *cry1* mutation with COP1OE and an antagonistic effect of CRY1OE with COP1OE in mediating blue-light responsiveness. 1, wild type (WS ecotype); 2, wild type (No-0 ecotype); 3, wild type (Ler ecotype); 4, *cry1* (*hy4-1*, Ler ecotype); 5, *cry1*/COP1OE; 6, COP1OE (No-0 ecotype); 7, CRY1OE (WS ecotype); and 8, CRY1OE/COP1OE. The scale bar represents about 2 mm. (**B**) A histogram compares the hypocotyl lengths of seedlings with various genetic backgrounds or combinations. The numbers on the *x* axis represent the same samples as in (A). The value is the average of 20 individual seedlings (6 days old), and the error bars represent the standard deviations. (**C**) The constitutive photomorphogenic (*cop*) and light-hypersensitive phenotypes of the GUS-CCTs transgenic seedlings (*15*). The top panels show dark-grown seedlings, and the bottom panels show blue light–grown seedlings (all in the Columbia ecotype). 1, wild type; 2, the GUS-CCT1 transgenic seedlings provided by A. R. Cashmore (*10*); 3, GUS-CCT1 transgenic seedlings generated in this study; 4, GUS-CCT2 transgenic seedlings generated in this study; and 5, *cop1-4* mutant. The scale bars in all panels represent about 1 mm. (**D**) A Western blot analysis probed with HY5 antibodies to show that dark-grown GUS-CCT1 and GUS-CCT2 transgenic seedlings accumulate HY5. Lane 1, wild type; lane 2, GUS-CCT1; and lane 3, GUS-CCT2. An equal amount of protein was loaded and verified by the intensity of a cross-reacting band (arrow).

blue light, comparable to the *cry1* mutants. Overexpressing CRY1 (CRY1OE) causes a hypersensitive response to blue light, and the seedlings display much-shortened hypocotyls and more expanded cotyledons. The *cry1*/COP1OE seedlings exhibit a much further reduced response to blue light–mediated hypocotyl growth inhibition than either *cry1* or the COP1OE parental seedlings. In addition, the hypersensitivity caused by CRY1OE is substantially reduced when combined with COP1OE.

To provide further functional evidence for the working hypothesis, we generated GUS-CCT1 and GUS-CCT2 transgenic plants and tested whether the activity of COP1 is affected in these transgenic seedlings. As reported previously (*10*), both transgenic seedlings exhibit a *cop*-like phenotype in the dark and are hypersensitive to light (Fig. 3C). In addition, we found a drastic accumulation of HY5 in both dark-grown transgenic seedlings when compared with dark-grown wild-type seedlings (Fig. 3D). Because HY5 degradation in darkness is a COP1-dependent process (*8*), this result suggests that the activity of COP1 is impaired in the GUS-CCTs seedlings and it is most plausible that the CCTs in the GUS fusion forms may repress COP1 activity by mimicking a light-activated conformation of the cryptochromes.

This scenario leads us to further predict that dark-grown GUS-CCTs transgenic seedlings should display a global genome expression profile similar to that of dark-grown *cop1* mutants. In addition, their profiles should mimic that of blue light–grown wild-type seedlings, as the two cryptochromes are the major photoreceptors for mediating blue light–controlled photomorphogenic development. To test these predictions, we examined the role of cryptochromes in mediating genome expression under blue light [both wild-type and the *cry1:cry2* double mutants (*19*)] and compared them with those of dark-grown *cop1-4* mutant (*5*), GUS-CCT1, and GUS-CCT2 seedlings using an *Arabidopsis* cDNA microarray (*22*).

As shown in Fig. 4A, the blue light–regulated genome expression profile in wild-type seedlings (lane 1) and the blue light effect mediated by the two cryptochromes (lane 2) are largely similar. Blue light could activate the phytochrome photoreceptors to a certain extent, which may contribute to the observed small difference between this pair

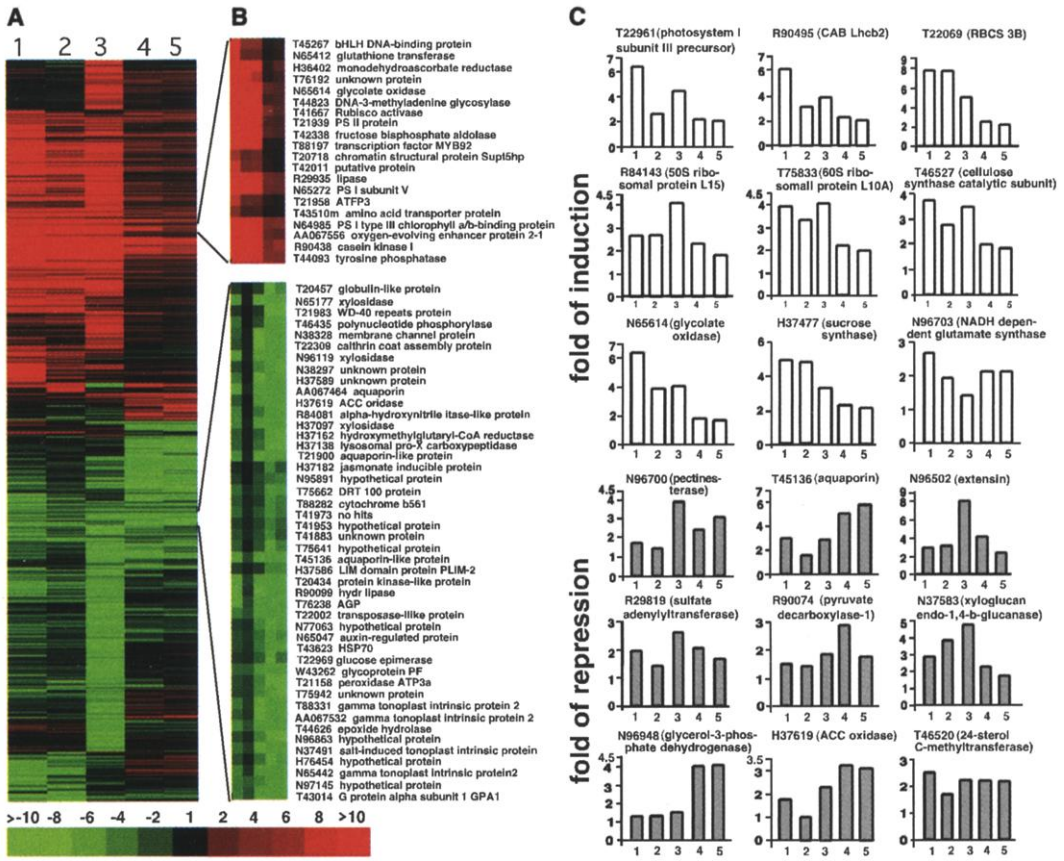

Fig. 4. Comparison of the global gene expression profiles of dark-grown GUS-CCTs transgenic and *cop1-4* seedlings with blue light–grown *cry1:cry2* double-mutant and wild-type seedlings (all in the Columbia ecotype) (*15*). (**A**) The overview of the hierarchical cluster display. Lane 1, expression ratios of blue light– and dark-grown wild-type seedlings (WT/B versus WT/D). Lane 2, expression ratios of blue light–grown wild-type and *cry1:cry2* double-mutant seedlings (WT/B versus *cry1:cry2*/B). Lane 3, expression ratios of dark-grown *cop1-4* and wild-type seedlings (*cop1-4*/D versus WT/D). Lane 4, expression ratios of dark-grown GUS-CCT1 transgenic and wild-type seedlings (GUS-CCT1/D versus WT/D). Lane 5, expression ratios of dark-grown GUS-CCT2 transgenic and wild-type seedlings (GUS-CCT2/D versus WT/D). A total of 3243 ESTs that have at least 2.0-fold differential expression in one of the five sample pairs are included in the cluster. (**B**) Two sample subclusters of ESTs displaying similar up- or down-regulation by blue light, two cryptochromes (CRY1 and CRY2), *cop1-4* mutation, and GUS-CCTs. (**C**) Representative examples of genes for selected pathways similarly up- or down-regulated in all five experimental pairs. The *y* axis values indicate the fold of induction or repression for gene expression. For raw data, see http://plantgenomics.biology.yale.edu/. The numbers on the *x* axis represent the five different sample pairs in the same order as shown in (A). The gene accession numbers and the proteins encoded are shown at the top of each panel.

of expression profiles. Further, the dark-grown *cop1-4* mutant seedlings indeed display a highly overlapping genome expression profile (lane 3) with that of blue light–grown wild-type seedlings. The global gene expression profiles of dark-grown GUS-CCT1 and GUS-CCT2 transgenic seedlings are essentially identical (lanes 4 and 5), despite the distinct CCT sequences (*17*), and are largely overlapping with those of dark-grown *cop1-4* and blue light–grown wild-type seedlings (Fig. 4, A and B). The *cop1-4* mutation seems to cause a stronger effect on the genome expression profile (both up- and down-regulated gene expression). However, much of the expression profile differences are quantitative, rather than qualitative in nature. We observed that up to 84% (886) of the expressed sequence tags (ESTs) up-regulated in the GUS-CCT1 seedlings are also up-regulated in the *cop1-4* mutant seedlings. Similarly, 82% (1122) of the ESTs down-regulated in the GUS-CCT1 seedlings are also repressed in the *cop1-4* mutant seedlings (*23*).

Many of the genes defined by those ESTs similarly regulated by blue light, GUS-CCTs, or the *cop1-4* mutation encode proteins involved in a large number of fundamental cellular processes or metabolic pathways associated with photomorphogenesis (*22*). A selected set of sample genes for representative cellular processes or metabolic pathways is shown in Fig. 4C. Some of the up-regulated genes encode enzymes for the photosynthetic light reaction components, enzymes implicated in the Calvin cycle, sucrose synthesis, amino acid biosynthesis, chloroplast and cytoplasmic protein translation machinery, photorespiration, and cell wall synthesis. The up-regulation of these genes and pathways leads to the production and export of carbohydrates from the chloroplast to the cytosol to provide energy and carbon sources for many biosynthetic pathways. On the other hand, many genes involved in sulfur assimilation, fatty acid β-oxidation, glyoxylate cycle, water transport, cell wall degradation, brassinosteroids, and ethylene biosynthesis are down-regulated. Particularly, the elongation of hypocotyl cells is dependent on cell wall relaxation and expansion and water influx into the cytosol and the vacuole compartments. The former is controlled by a series of cell wall loosening/hydrolytic enzymes (*24*), and the latter is controlled by water channel proteins (aquaporins) (*25*). The coordinated regulation of expression for these genes and pathways should contribute to the morphological characteristics of light-grown photomorphogenic seedlings and account for the *cop* phenotype of dark-grown *cop1* mutant and the GUS-CCTs transgenic seedlings.

Our finding that light-activated cryptochromes repress COP1 activity through a direct protein-protein interaction, together with the observed *cop*-like phenotype of the GUS-CCTs transgenic seedlings, provides supporting evidence for the "intramolecular redox model" of cryptochrome function (*10*). In addition, the direct physical association between cryptochromes and the downstream photomorphogenesis repressor COP1 may help to explain the fact that no blue/UV-A light–specific signaling components (except the photoreceptors themselves) have been identified in extensive genetic screens so far. Such a direct and short signaling mechanism for both cryptochromes is conceptually very efficient, through which gene expression and developmental program can be readily modulated.

References and Notes

1. X. W. Deng, P. H. Quail, *Semin. Cell Dev. Biol.* **10**, 121 (1999).
2. A. R. Cashmore, J. A. Jarillo, Y.-J. Wu, D. Liu, *Science* **284**, 760 (1999).
3. X. W. Deng *et al.*, *Cell* **71**, 791 (1992).
4. N. Wei, X. W. Deng, *Plant Physiol.* **112**, 871 (1996).
5. L.-H. Ang, X. W. Deng, *Plant Cell* **6**, 613 (1994).

6. T. Oyama, Y. Shimula, K. Okada, *Genes Dev.* **11**, 2983 (1997).
7. S. Chattopadhyay, L.-H. Ang, P. Puente, X. W. Deng, N. Wei, *Plant Cell* **10**, 673 (1998).
8. M. T. Osterlund, C. Hardtke, N. Wei, X. W. Deng, *Nature* **405**, 462 (2000).
9. N. Wei, X. W. Deng, *Trends Genet.* **15**, 98 (1999).
10. H.-Q. Yang *et al.*, *Cell* **103**, 815 (2000).
11. G. Serino *et al.*, *Plant Cell* **11**, 1967 (1999).
12. T. W. McNellis, A. G. von Arnim, X. W. Deng, *Plant Cell* **6**, 1391 (1994).
13. H. Guo, H. Duong, N. Ma, C. Lin, *Plant J.* **19**, 279 (1999).
14. L.-H. Ang *et al.*, *Mol. Cell* **1**, 213 (1998).
15. Web fig. 1 and experimental details can be viewed at *Science* Online at www.sciencemag.org/cgi/content/full/1063630/DC1.
16. M. Holm, X. W. Deng, *Plant Mol. Biol.* **41**, 151 (1999).
17. M. T. Osterlund, L.-H. Ang, X. W. Deng, *Trends Cell Biol.* **9**, 113 (1999).
18. C. Lin *et al.*, *Proc. Natl. Acad. Sci. U.S.A.* **95**, 2686 (1998).
19. T. C. Mockler, H. Guo, H. Yang, H. Duong, C. Lin, *Development* **126**, 2073 (1999).
20. C. Lin, M. Ahmad, A. R. Cashmore, *Plant J.* **10**, 893 (1996).
21. M. Ahmad, A. R. Cashmore, *Nature* **366**, 162 (1993).
22. L. Ma *et al.*, *Plant Cell*, in press.
23. We chose 1.25 and 0.8 as the cutoff ratios to group ESTs as up- or down-regulated, respectively, by the *cop1-4* mutation and GUS-CCT1, because they represent substantial and reproducible differences in the levels of mRNA in our experiments.
24. D. J. Cosgrove, *Plant Physiol.* **125**, 13 (2001).
25. C. Maurel, M. J. Chrispeels, *Plant Physiol.* **125**, 135 (2001).
26. We thank C. Lin for providing the CRY2 antibody, A. R. Cashmore for providing a GUS-CCT1 transgenic line, and T. Nelson for critical reading and comments on the manuscript. This work was supported by a NIH grant (GM-47850) to X.W.D. and a NIH grant (GM59507) to H.Y.Z. H.W. is a NIH postdoctoral fellow and X.W.D. was a NSF Presidential Faculty Fellow.

20 June 2001; accepted 7 August 2001
Published online 16 August 2001;
10.1126/science.1063630
Include this information when citing this paper.

Conversion of a Peroxiredoxin into a Disulfide Reductase by a Triplet Repeat Expansion

Daniel Ritz,[1] Jackie Lim,[1] C. Michael Reynolds,[2] Leslie B. Poole,[2] Jon Beckwith[1]*

Pathways for the reduction of protein disulfide bonds are found in all organisms and are required for the reductive recycling of certain enzymes including the essential protein ribonucleotide reductase. An *Escherichia coli* strain that lacks both thioredoxin reductase and glutathione reductase grows extremely poorly. Here, we show that a mutation occurring at high frequencies in the gene *ahpC*, encoding a peroxiredoxin, restores normal growth to this strain. This mutation is the result of a reversible expansion of a triplet nucleotide repeat sequence, leading to the addition of one amino acid that converts the AhpC protein from a peroxidase to a disulfide reductase. The ready mutational interconversion between the two activities could provide an evolutionary advantage to *E. coli*.

The cytoplasms of all living cells are highly reducing environments compared with their external milieu. A host of cytosolic proteins are responsible for maintaining a redox balance. In *E. coli*, two pathways in the cytoplasm function in overlapping ways to maintain cysteine residues in the reduced state (*1*). The thioredoxin system includes thioredoxin reductase (*trxB*) and two thioredoxins; the glutaredoxin system includes glutathione reductase (*gor*), glutathione, and three glutaredoxins (*2, 3*). These two systems recycle certain reductive enzymes by reducing disulfide bonds formed at their active sites (*4–7*).

A *trxB,gor* double mutant, lacking both cytosolic disulfide reductive pathways, grows poorly under aerobic conditions unless a reducing agent such as dithiothreitol (DTT) is present. The poor growth is likely due to the inability of these cells to synthesize deoxyribonucleotides, because ribonucleotide reductase is not maintained in the reduced state.

We have previously described a derivative of the *trxB,gor* mutant strain, FÅ113, in which a suppressor mutation has restored a normal growth rate (*8*). Despite the likelihood that a source of disulfide-reducing power has been restored by the suppressor mutation, FÅ113 is able to efficiently catalyze disulfide bond formation in cytoplasmically retained secreted proteins. FÅ113 and its derivatives also enhance the expression in the cytoplasm of active tissue plasminogen activator (vtPA), a complex eukaryotic protein with multiple disulfide bonds (*8*).

We wished to determine the nature of the suppressor mutation in FÅ113. However, even though the cells were grown in the presence of DTT, suppressors arose in this strain at such a high frequency that we could not map them using transposon insertions that were cotransduced by bacteriophage P1 with the suppressor mutation. To overcome this problem, we introduced into the *trxB,gor* mutant a plasmid that contained the *trxB* gene under the control of the pBAD *ara* promoter (*9*). The frequency of suppressor mutations that occurred under restrictive growth conditions was still 0.5×10^{-3}. Transposon insertions linked to the suppressor mutation clustered to minute 14 of the *E. coli* chromosome, and the linkage data suggested that a mutation in the *ahpCF* locus might be responsible for the suppression (Fig. 1A).

The *ahpCF* locus of *E. coli* encodes the alkyl hydroperoxidase system, which reduces both hydrogen peroxide and alkyl hydroperoxides, thus protecting the cells from oxidative damage. Peroxides oxidize the active site Cys^{46} of the AhpC dimer to a sulfenic acid intermediate that is converted to a disulfide bond when it is attached by Cys^{165} in the other subunit of the homodimer (*10*). The mechanism of reductive electron transfer in the AhpCF system involves a cascade of disulfide bond reduction steps. First, electrons are transferred from NADH via a flavin moiety in the COOH-terminus of AhpF to reduce a disulfide bond in that portion of the protein. The electrons from these reduced cysteines are then donated to a disulfide bond in the NH_2-terminal domain of AhpF (*11*), from which they are transferred to the disulfide bond in AhpC, regenerating the reduced active form of the protein (*12, 13*).

Sequence analysis of the entire *ahpCF* locus from the wild-type, FÅ113, and nine independently isolated suppressor strains revealed that all of the mutants contained the same mutation, an insertion of three bases (TCT) after base 103 of the *ahpC* coding region (Fig. 1B). The wild-type gene contains four direct repeats of TCT, whereas the mutants contain five. This change results in the addition of a single amino acid (Phe^{38}), located only nine amino acids away from the active site Cys^{46} (Fig. 1B). We refer to the mutant protein as AhpC*.

Expansion of a repeated sequence, as is found in the *ahpC** mutation, is usually a very frequent event (*14*) and would explain the finding that all the suppressors represent

[1]Department of Microbiology and Molecular Genetics, 200 Longwood Avenue, Harvard Medical School, Boston, MA, 02115, USA. [2]Department of Biochemistry, Wake Forest University School of Medicine, Winston-Salem, NC, 27157, USA.

*To whom correspondence should be addressed. E-mail: jon_beckwith@hms.harvard.edu